

# Rossby Wave Breaking and Transient Eddy Forcing during Euro-Atlantic Circulation Regimes

ERIK T. SWENSON

*Center for Ocean–Land–Atmosphere Studies, George Mason University, Fairfax, Virginia*

DAVID M. STRAUS

*Department of Atmospheric, Oceanic, and Earth Sciences, College of Science, George Mason University, Fairfax, Virginia*

(Manuscript received 9 September 2016, in final form 24 February 2017)

## ABSTRACT

The occurrence of boreal winter Rossby wave breaking (RWB) along with the quantitative role of synoptic transient eddy momentum and heat fluxes directly associated with RWB are examined during the development of Euro-Atlantic circulation regimes using ERA-Interim. Results are compared to those from seasonal reforecasts made using the Integrated Forecast System model of ECWMF coupled to the NEMO ocean model. The development of both Scandinavian blocking and the Atlantic ridge is directly coincident with anticyclonic wave breaking (AWB); however, the associated transient eddy fluxes do not contribute to (and, in fact, oppose) ridge growth, as indicated by the local Eliassen–Palm (EP) flux divergence. Evidently, other factors drive development, and it appears that wave breaking assists more with ridge decay. The growth of the North Atlantic Oscillation (NAO) in its positive phase is independent of RWB in the western Atlantic but strongly linked to AWB farther downstream. During AWB, the equatorward flux of cold air at upper levels contributes to a westerly tendency just as much as the poleward flux of momentum. The growth of the negative phase of the NAO is almost entirely related to cyclonic wave breaking (CWB), during which equatorward momentum flux dominates at jet level, yet low-level heat fluxes dominate below. The reforecasts yield realistic frequencies of CWB and AWB during different regimes, as well as realistic estimates of their roles during development. However, a slightly weaker role of RWB is simulated, generally consistent with a weaker anomalous circulation.

## 1. Introduction

Rossby wave breaking (RWB) is a fundamental atmospheric process that bridges climate variability with extreme weather (McIntyre and Palmer 1983; Ryoo et al. 2013; Liu and Barnes 2015). Because RWB is generally associated with significant poleward transport of momentum, heat, and moisture, dynamical misrepresentation of RWB may lead to the deterioration of long-range prediction skill and an increase of uncertainty in long-term projections. Thus, it is essential to not only have a clear understanding of the interactive role of RWB in driving the circulation, but also to identify limitations of dynamical models in representing RWB.

RWB typically occurs when a Rossby wave reaches sufficient amplitude and/or encounters jet exit regions

over the Pacific and Atlantic basins. RWB is identified by overturning in potential vorticity and irreversible mixing associated with the return of momentum from transient eddies to the mean flow. Cyclonic wave breaking (CWB) primarily occurs on the poleward flank of jet exit regions, whereas anticyclonic wave breaking (AWB) tends to occur farther equatorward and downstream of jet exit regions (Martius et al. 2007; Strong and Magnusdottir 2008). CWB and AWB significantly alter upper-tropospheric jets. Equatorward momentum fluxes associated with CWB and poleward momentum fluxes associated with AWB play an important role in the life cycle of baroclinic waves (Balasubramanian and Garner 1997). RWB is observed to modulate the weather in how it affects the formation of blocking (Pelly and Hoskins 2003; Masato et al. 2013) and atmospheric rivers (Ryoo et al. 2013). RWB is also associated with intense transport of moisture into the Arctic (Liu and Barnes 2015). Remote tropical forcing associated with the El Niño–Southern Oscillation (ENSO)

---

*Corresponding author e-mail:* Erik T. Swenson, eswenso1@gmu.edu

and the Madden–Julian oscillation (MJO) are observed to impact the frequency and location of RWB (Moore et al. 2010; Drouard et al. 2015; MacRitchie and Roundy 2016), while the wave breaking itself presumably plays a significant role in the associated midlatitude responses.

Given the potentially significant synoptic transient eddy forcing of the low-frequency or time-mean flow that occurs in association with RWB, there has been interest in determining how RWB affects large-scale circulation regimes and their transitions. In particular, observed changes in RWB frequency directly associated with the prominent intraseasonal Euro-Atlantic circulation regimes and their transitions have been studied by Strong and Magnusdottir (2008), Cassou (2008), Michel and Rivière (2011), and Franzke et al. (2011). The relationship between RWB and the North Atlantic Oscillation (NAO) has been studied from a kinematic point of view (Benedict et al. 2004; Franzke et al. 2004). The meridional transport of zonal momentum and its convergence has been identified as one component of the RWB-related synoptic forcing (see, e.g., Cassou 2008) following the “tilted trough” concept (Machta 1949; Lorenz 1963). In addition, the synoptic forcing has been identified using single-level vorticity budgets, as in Michel and Rivière (2011). Rivière and Orlanski (2007) infer the role of RWB for the NAO by examining transient eddy momentum and heat fluxes but do not quantify the relative impact of both these fluxes on the circulation. Potential vorticity couples both the vorticity and thermodynamic equations via vertical velocity (Lau and Holopainen 1984). A full reckoning of the three-dimensional baroclinic transient eddy forcing of the low-frequency flow also involves the meridional flux of sensible heat and its vertical derivative (Holopainen et al. 1982; Plumb 1986; Trenberth 1986). There has been much less emphasis on understanding this component of the full forcing.

This study aims to estimate the role of RWB in terms of both the climatological mean and with respect to different Euro-Atlantic circulation regimes. We assess the full baroclinic transient eddy forcing (as a result of both momentum and heat fluxes) in terms of the portion that is directly related to RWB as well as that which is independent of RWB (how important is RWB?). We also examine how well RWB and the associated transient eddy forcing are simulated by climate models. Whether or not increasing horizontal resolution affects model representation of this is an additional question of interest.

## 2. Data and methods

### a. Reforecast and reanalysis data

In this study, multiple reforecast (or seasonal hindcast) datasets are examined from Project Minerva (see

Zhu et al. 2015; Manganello et al. 2016). The Integrated Forecast System (IFS) of the European Centre for Medium-Range Weather Forecasts (ECMWF) is run at a range of horizontal resolutions, with a fixed vertical resolution of 91 levels. The IFS is coupled with the Nucleus for European Modeling of the Ocean (NEMO) in a configuration similar to that of System 4 (Molteni et al. 2011). In particular, the horizontal resolution of NEMO is  $1^\circ$  but is refined to nearly  $\frac{1}{3}^\circ$  near the equator. Reforecasts are produced at an atmospheric horizontal resolution of about 62 km ( $0.56^\circ$ ), 31 km ( $0.28^\circ$ ), and 16 km ( $0.14^\circ$ ) along the equator, corresponding to triangular truncations of T319, T639, and T1279, respectively. For each year spanning 1980–2010, 15 ensemble members are initialized on 1 November and run for 7 months. The ERA-Interim (hereinafter, ERAI; Dee et al. 2011) is used as a corresponding observationally constrained dataset, which is defined on the native  $512 \times 256$  Gaussian grid with a horizontal resolution of roughly 77 km ( $0.7^\circ$ ) along the equator, corresponding to a triangular truncation of T255.

Daily mean isentropic Ertel potential vorticity (PV) is used for the detection of Rossby wave breaking. PV is analyzed on original resolution grids for both the reforecasts and ERAI. We use once-daily fields for analyses of other variables. At 11 pressure levels, geopotential height, temperature, and horizontal winds from ERAI are available on a high-resolution Gaussian grid. These fields are transformed into spectral space, truncated to T42 spectrally, and expressed on a  $128 \times 64$  (longitude by latitude) grid. For the Minerva reforecasts, these fields are available in spectral space (i.e., as spherical harmonic coefficients for the resolutions of T319, T639, and T1279). The fields are truncated to a T42 spherical harmonic representation and expressed on the same  $128 \times 64$  grid. The climatological seasonal cycle of each field is computed by fitting a parabola to the time series at each grid point for the period of November through mid-April, and then averaging the parabolic fit over all years. [A parabola is an efficient way to represent the annual cycle over one season without requiring data from other seasons (see Straus 1983).] Anomalies are further filtered into low-frequency (periods greater than 10 days) and high-frequency (periods less than or equal to 10 days) components (see Straus 2010). The resultant filtered data are analyzed for the 136-day boreal winter season (16 November–31 March, or 30 March on leap years). Low-frequency 500-hPa geopotential height (Z500) is used for the cluster analysis, while the high-frequency temperature and wind fields are used for the calculation of the transient eddy forcing of the mean flow.

### *b. Circulation regimes*

Circulation regimes are computed from the low-frequency anomalous Z500 over the Euro-Atlantic region: 20°–90°N, 90°W–30°E. This region is chosen to be consistent with a number of earlier studies (e.g., Vautard 1990; Cassou 2008), but regimes have little sensitivity to modest changes in the domain. The regimes are identified using a cluster analysis based on the *k*-means partitioning algorithm, as described in Michelangeli et al. (1995), Straus et al. (2007), and Straus (2010). A choice of 4 distinct clusters is made based on significance at the 95% confidence level determined from a Monte Carlo procedure. For details of the cluster analysis and significance, please see appendix A. Consistent with past studies (e.g., Vautard 1990; Cassou 2008), the robust patterns include Scandinavian blocking, the Atlantic ridge, and both positive and negative phases of the North Atlantic Oscillation. The dynamical state associated with each cluster is assessed by compositing fields according to days that the circulation belongs to each cluster.

### *c. Rossby wave breaking*

Rossby wave breaking (RWB) is defined here by regions of overturning, or streamers, of PV along isentropic surfaces in the upper troposphere (namely 315 and 330 K). The direction of overturning is distinguished as cyclonic or anticyclonic, corresponding to the breaking stage of wave life cycles identified by Thorncroft et al. (1993). Isentropic PV is used because it is conserved in the absence of nonadiabatic processes, such as latent heating, allowing for a more straightforward interpretation as a tracer. The objective detection of RWB follows in part the analysis made by Strong and Magnusdottir (2008); however, the exact definition of area of overturning differs, and an additional constraint related to the gradient in PV is used. To retain narrow features involved with filamentation, PV is analyzed at its native grid resolution with only very small-scale smoothing applied prior. Details of the algorithm are described in appendix B.

Concerning vertical sensitivity, CWB tends to exhibit frequency maxima near 315 K, whereas AWB tends to exhibit maxima at a relatively higher level, near 330 K. For ERAI, note that the climatological frequencies of CWB and AWB computed at these levels are quite consistent with that computed in terms of potential temperature at 2 PVU (not shown); however, the latter is found to be much more sensitive to the constraint on gradient because of relatively weaker gradients in potential temperature.

Considering that consistency with the Minerva reforecasts is essential, daily mean PV is also used for ERAI. An approximation is made by daily averaging 6-hourly instantaneous data. Given that many breaking episodes last for a short time, it is found that daily averaging systematically reduces estimates of RWB frequency (not shown). For instance, RWB is estimated to be much more frequent if examined using instantaneous PV sampled once daily.

## 3. Climatological RWB

The climatological seasonal-mean frequency of CWB and AWB in ERAI exhibits distinct maxima (Fig. 1) in both the 315- and 330-K levels. The North Atlantic and western Europe are dominated by AWB (e.g., on average the United Kingdom tends to experience roughly 18 days of AWB during the winter season yet only a day or two of CWB). A weaker secondary maximum in AWB is found over western North America. The maximum frequency of AWB is comparable between levels; however, the geographic position is shifted poleward and eastward at 315 K compared with that at 330 K. On the other hand, maxima in CWB frequency are located poleward and westward of these regions near the southern tip of Greenland and around the Bering Sea. Here CWB is generally twice as frequent at 315 K compared with that at 330 K, and roughly two weeks (one week) are characterized by CWB at the 315-K (330-K) level during the winter season. Note also that maxima in the frequency of CWB and AWB are significantly reduced in terms of PV at 350 K (not shown). The vertical sensitivity of RWB frequency is consistent with that found by Martius et al. (2007), although systematic differences in the latitude of maximum AWB result from differing definitions of PV streamers [contrast Fig. 1 with Fig. 5 of Martius et al. (2007)]. Coincident with maintenance of the eddy-driven jets, AWB maxima are located slightly downstream of climatological jet exit regions, while CWB maxima are found farther upstream along the poleward flanks of jet exit regions. The direct association between wave breaking and the climatological jet is shown at the end of this section.

The corresponding seasonal frequency of RWB is shown for the Minerva reforecasts (further averaged across 15 ensemble members) in Fig. 2. Note that a low-latitude spike in AWB frequency near 120°E is simply an artifact of the Himalayas, although it appears more pronounced in the reforecasts. The patterns of climatological CWB and AWB are quite similar to those identified in ERAI, and maxima are well simulated by the IFS run across the range of horizontal resolutions.

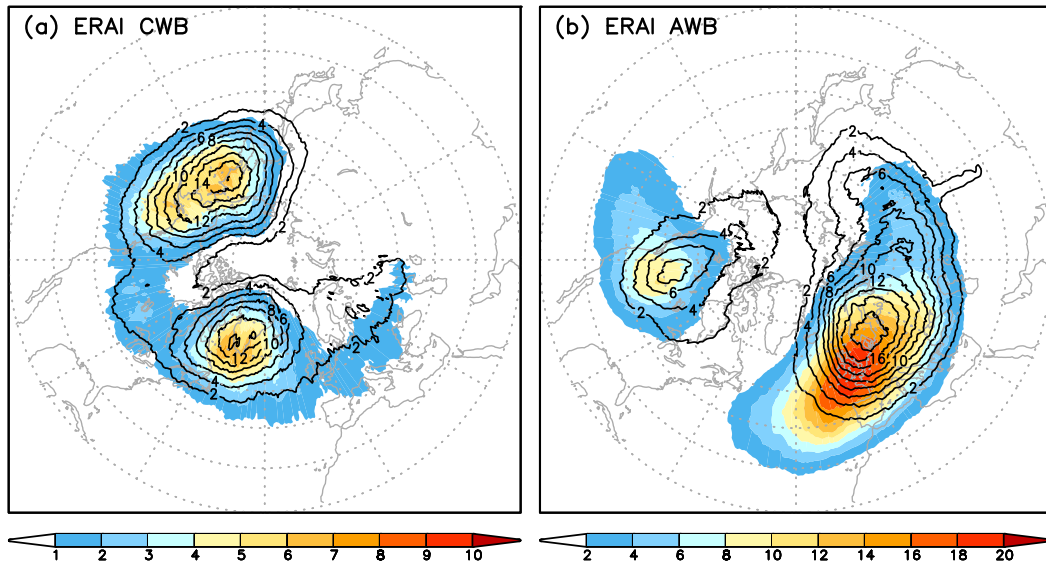


FIG. 1. Climatological seasonal frequency (days per season) of (a) CWB and (b) AWB, computed for ERAI in terms of PV at 330 (shading) and at 315 K (contours) over the Northern Hemisphere ( $20^{\circ}$ – $90^{\circ}$ N). Boreal winter (16 Nov–31 Mar) spanning 1980/81–2010/11 is used. Note that the scale of AWB is twice that of CWB at 330 K.

There is, however, a slight underestimation in frequency of occurrence: both CWB and AWB are simulated to occur roughly 1–5 days less than that found in ERAI. These differences may be found by examining RWB frequency for any individual ensemble member alone. Such a bias could possibly be the result of the IFS being overly diffusive, either dynamically or as a consequence of convective parameterization. Interestingly, increasing horizontal resolution does not improve the frequency of wave breaking events, and results for the lowest resolution reforecasts (T319) actually yield the largest estimates that are closest to ERAI. For the remaining analyses presented in this study, differences between results for the Minerva reforecasts run at different resolutions are fairly small; thus, the following results are shown only for Minerva T1279. We hereinafter refer to Minerva T1279 as “Minerva” unless otherwise specified.

CWB and AWB directly modify the path of transient eddies and, more importantly, their associated momentum and heat fluxes, consequently altering the slowly evolving circulation. Here we quantify the direct association between RWB and upper-tropospheric zonal wind by partitioning variability into that related to CWB, that related to AWB, and that not related to RWB. For an individual CWB or AWB event detected on a given day with a centroid (average geographic position of all grid points of streamer) and areal extent with equivalent radius  $R$ , simultaneous variations in local wind and temperature within a distance of  $4R$  of the centroid are considered to be directly related to the breaking event, whereas variations occurring outside of

this range are considered to be independent (non-RWB). Attribution is made for events detected at either 315 or 330 K or both. See appendix C for further details regarding associating variability with CWB and AWB, as well as for centroid-centered composite results for ERAI.

To diagnose the impact of synoptic transient eddies on the more slowly evolving zonal flow, we compute the divergence of the local three-dimensional Eliassen–Palm (EP) flux (Trenberth 1986). In principle, the divergence represents the forcing of these transient eddies on the time-mean zonal wind (as a tendency), where the time mean is defined as a period sufficiently long compared to the time scale of the transient eddies (10 days or less). The EP flux divergence is given by

$$\begin{aligned} \nabla \cdot \mathbf{E} &= \left[ \frac{\cos\phi}{2} \frac{\partial}{\partial x} (\overline{v'^2} - \overline{u'^2}) - \frac{\partial}{\partial y} (\overline{u'v'} \cos\phi) \right] \\ &+ \left[ -\cos\phi \frac{\partial}{\partial p} \left( R_d f p \frac{\overline{v'T'}}{S} + \overline{u'w'} \right) \right] \\ &= \nabla \cdot \mathbf{E}_H + \nabla \cdot \mathbf{E}_V, \end{aligned} \quad (1)$$

where primes denote high-frequency components (periods  $\leq 10$  days) and overbars denote time averaging. Equation (1) involves temperature  $T$ , zonal wind  $u$ , meridional wind  $v$ , pressure vertical velocity  $w$ , latitude  $\phi$ , the Coriolis parameter  $f$ , pressure  $p$ , static stability  $S = R_d(\partial\overline{T}/\partial z + \kappa\overline{T})$ , gas constant  $R_d = 287 \text{ J kg}^{-1} \text{ K}^{-1}$ , and  $\kappa = 0.286$ . We interpret the high-frequency components as representing the baroclinically active systems in storm tracks (Wallace et al. 1988). Note that Eq. (1)

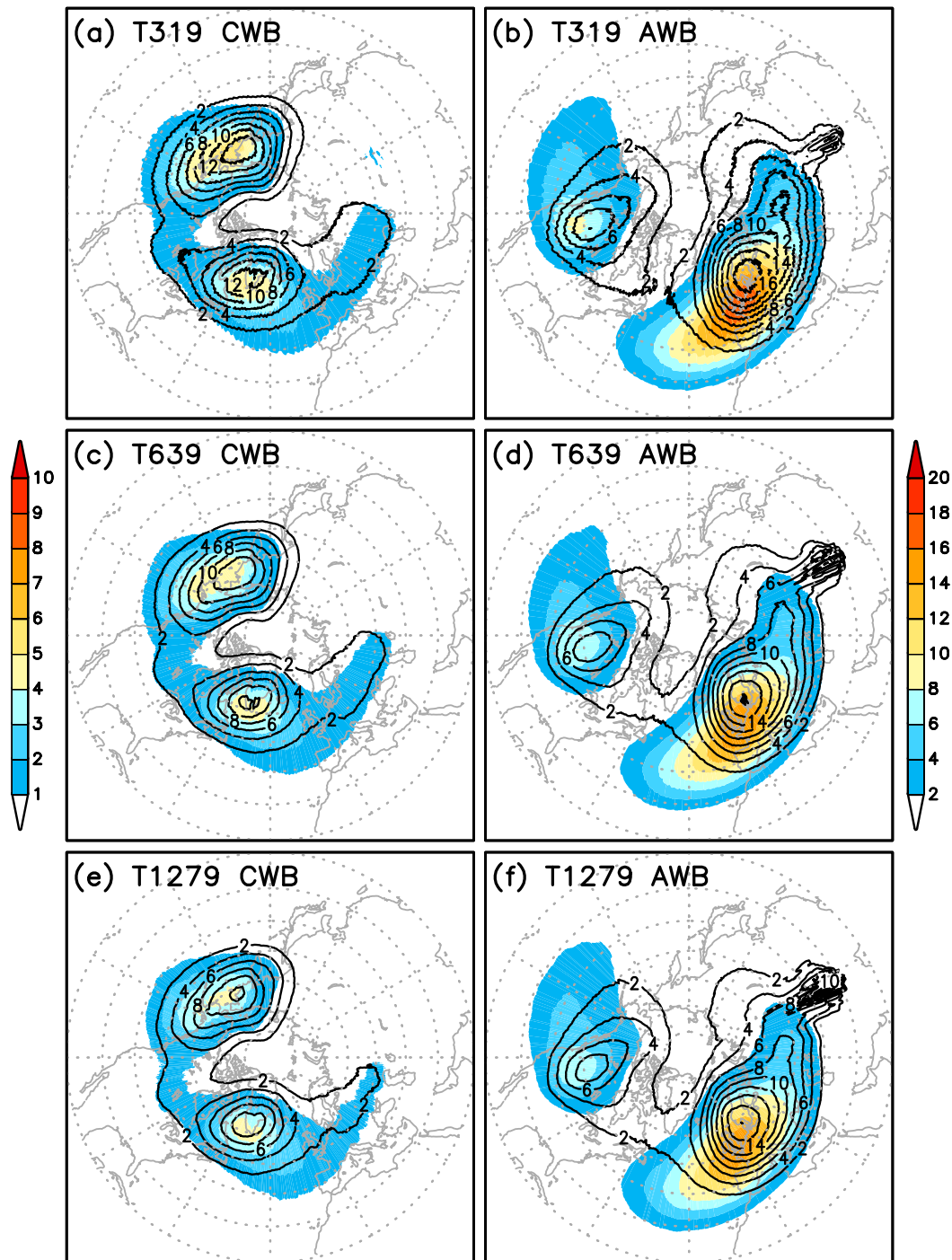


FIG. 2. As in Fig. 1, but for Minerva reforecasts run at (a),(b) T319; (c),(d) T639; and (e),(f) T1279 spectral resolution. Results are further averaged over 15 ensemble members.

results from taking the divergence of the zonal component of the local EP flux given by Eq. (A12) of Trenberth (1986), and expressing the vertical term as a function of pressure. The first term ( $\nabla \cdot \mathbf{E}_H$ ) quantifies the impact from transient eddy horizontal momentum

fluxes, while the second term ( $\nabla \cdot \mathbf{E}_V$ ) gives the vertical component, which is generally dominated by the impact of transient heat fluxes. [The role of the vertical momentum fluxes is relatively small; without it, Eq. (1) represents the quasigeostrophic impact of the transient

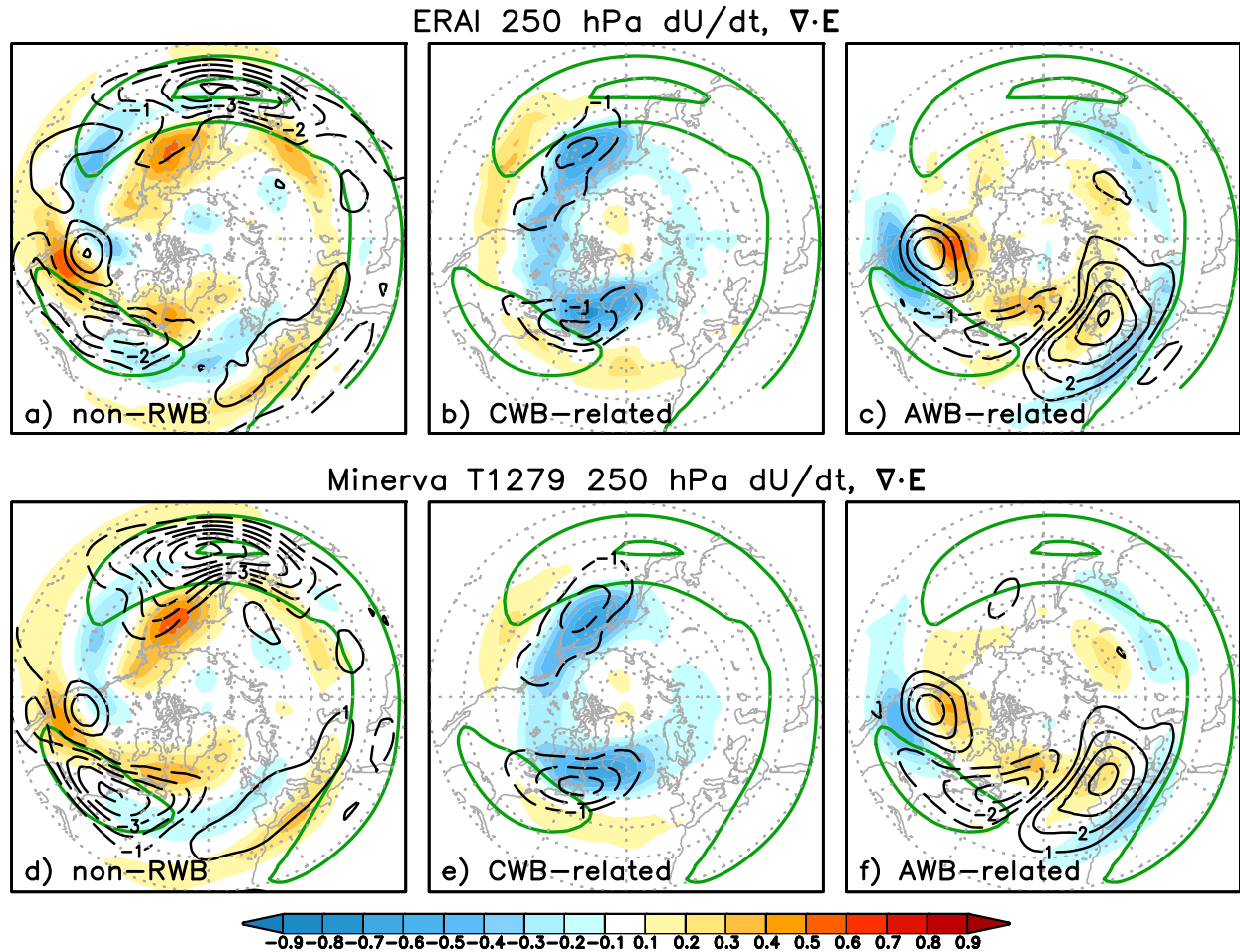


FIG. 3. Climatological zonal wind tendency (shading;  $\text{m s}^{-1} \text{ day}^{-1}$ ) and divergence of the local EP flux ( $\nabla \cdot \mathbf{E}$ ; contours;  $\text{m s}^{-1} \text{ day}^{-1}$ ) at 250 hPa over the Northern Hemisphere ( $20^{\circ}$ – $90^{\circ}\text{N}$ ). Results are partitioned according to the tendency (left) not associated with RWB, (center) associated with CWB, or (right) associated with AWB for (a)–(c) ERA1 and for (d)–(f) Minerva T1279. The total climatological zonal wind is also shown in green contours (at  $30$  and  $60 \text{ m s}^{-1}$ ).

eddies.] We focus on large-scale features by truncating fields of EP flux divergence to T21 spectral resolution.

Equation (1) provides a generalization of the transient eddy–zonal mean flow interaction to the local zonal flow. The transient eddies can indirectly impact the zonal wind through low-frequency meridional circulations (see Trenberth 1986), an effect that is not accounted for here. Equation (1) further neglects the impact of low-frequency terms involving advection and flux convergence, as well as the impact of diabatic heating and friction. By partitioning the full divergence given in Eq. (1) into wave-breaking-related contributions, we diagnose the contribution of synoptic transient eddies to the mean zonal wind tendency during various conditions. Since the total mean wind tendency is, by definition, very small, a positive contribution during AWB generally must be offset by corresponding negative contributions either during CWB or when RWB is

absent or by contributions from processes not directly related to the baroclinic transients and so not represented by Eq. (1).

Most studies to date assume or crudely infer the role of CWB and AWB by only examining average changes in frequency. To our knowledge, a similarly rigorous approach has not been taken previously toward quantifying the direct covarying role of RWB for driving circulation changes. Liu and Barnes (2015) apply a qualitatively similar method but examine the role of RWB for moisture transport. Some studies investigate the role of wave breaking but focus on a perspective relative to individual breaking events and neglect the effect of vertical variation of the meridional heat fluxes (e.g., Strong and Magnusdottir 2008; Wang and Magnusdottir 2011).

Figure 3 shows the non-RWB, CWB-related, and AWB-related climatological components of zonal wind

tendency and the divergence of the local EP flux ( $\nabla \cdot \mathbf{E}$ ) at 250 hPa for ERAI and Minerva. Independent of wave breaking, transient eddies provide an easterly forcing along Pacific and Atlantic jets that extends poleward near jet exit regions. This feature is simulated to be a bit stronger in Minerva than in ERAI. Transient eddies also provide an easterly forcing along the poleward flanks of jet exit regions during CWB, as well as during AWB over the Atlantic. As is shown later in [section 4d](#) for the Atlantic, the negative  $\nabla \cdot \mathbf{E}$  is primarily due to heat fluxes ( $\nabla \cdot \mathbf{E}_V$  is dominant) that operate to smooth the local horizontal temperature gradient and decelerate the jet via thermal wind. In the absence of wave breaking ([Fig. 3a](#)), corresponding easterly tendencies are fairly weak and shifted eastward relative to the regions of negative  $\nabla \cdot \mathbf{E}$ , whereas westerly tendencies are found to the north, indicative of a poleward shift in the jet. In the northern Atlantic, these westerly wind tendencies are also seen during AWB ([Fig. 3c](#)). During AWB,  $\nabla \cdot \mathbf{E}$  works against the westerly tendency in the northern Atlantic but supports this tendency in the eastern Atlantic/western Europe. This discrepancy between zonal wind tendency and  $\nabla \cdot \mathbf{E}$  reflects the impact of terms not accounted for by  $\nabla \cdot \mathbf{E}$ . A strengthening jet to the north is consistent with the tightening of the meridional temperature gradient in response to transient heat fluxes that occur to the south ([Simmons and Hoskins 1978](#)). However, keep in mind that low-frequency terms involved in any such adjustment process are not accounted for. Additionally, the time-mean diabatic heating is also known to overcompensate for the thermal effect of the transient eddies, thereby anchoring the position of climatological storm tracks ([Hoskins and Valdes 1990](#)). However, the easterly forcing from transient eddies does reinforce easterly wind tendencies during CWB, suggesting that such effects that are not accounted for by  $\nabla \cdot \mathbf{E}$  do not oppose zonal wind tendencies as much during CWB.

CWB and AWB have very different roles in directly maintaining the poleward-tilting eddy-driven jets ([Figs. 3b,c](#)). Over the northern Pacific and Atlantic basins, CWB is characterized by an equatorward shift in the jet for which easterlies are reinforced by transient eddies. Farther downstream, AWB is characterized by poleward movement of the jet for which westerlies are generally reinforced by transient eddies, evident in a broad area of positive  $\nabla \cdot \mathbf{E}$  over the eastern Atlantic and western Europe, as well as for a smaller region over western North America. The relative roles of CWB and AWB are reproduced quite well in Minerva, with some small biases. The  $\nabla \cdot \mathbf{E}$  maximum related to AWB over western Europe appears to be slightly underestimated, whereas the minimum upstream over the northern

Atlantic is slightly overestimated. There is evidence in ERAI and Minerva that variations in the subtropical jet over Saharan Africa are significantly linked with AWB (not shown). Later, we show that, although the pattern of the zonal wind tendency is largely consistent with the impact of transient horizontal momentum fluxes ( $\nabla \cdot \mathbf{E}_H$ ), quantitative  $\nabla \cdot \mathbf{E}$  calculations suggest that transient heat fluxes have a comparable if not dominant role (via  $\nabla \cdot \mathbf{E}_V$ ) during CWB and AWB, climatologically and during both phases of the NAO (see [sections 4c](#) and [4d](#)).

Only the simultaneous link with CWB and AWB is presented in this study, and given that wave breaking events tend to be short-lived, the associated temporal averaging tends to be somewhat fragmented. The climatological  $\nabla \cdot \mathbf{E}$  associated with CWB and AWB is found to be generally unchanged when a small time lag is included in attribution; however, interestingly, there are slightly stronger zonal wind tendencies prior to CWB and AWB (not shown).

#### 4. Relationship between RWB and Euro-Atlantic regimes

The distinct Euro-Atlantic circulation regimes identified in ERAI consist of Scandinavian blocking, the Atlantic ridge, and both positive and negative phases of the North Atlantic Oscillation (NAO+ and NAO−, respectively). These patterns in Z500 are reproduced quite well in the Minerva reforecasts run at all resolutions (not shown; see [Fig. 4](#) for both ERAI and Minerva T1279). Here we examine the changes in CWB and AWB associated with the different regimes, for which results are generally consistent with [Michel and Rivière \(2011\)](#). Given that PV variations are generally similar at 315 and 330 K, we present results in terms of CWB and AWB frequency averaged between both levels. We also quantify the relative roles of CWB and AWB during the developmental phase of each regime. This is defined to occur on the days when anomalous Z500 has an increasing pattern correlation with its associated regime pattern. The decay phase (defined with decreasing pattern correlation) is also considered for each regime and tends to span about the same number of days as development.

##### a. Scandinavian blocking

Scandinavian blocking is dominated by high mid-tropospheric height anomalies centered over the coast of Norway ([Fig. 4](#)). Around this region, [Masato et al. \(2013\)](#) find a maximum in the occurrence of blocking (distinct from a secondary maximum found near Greenland that is coincident with high height anomalies during the NAO−). The ridge over northern Europe is

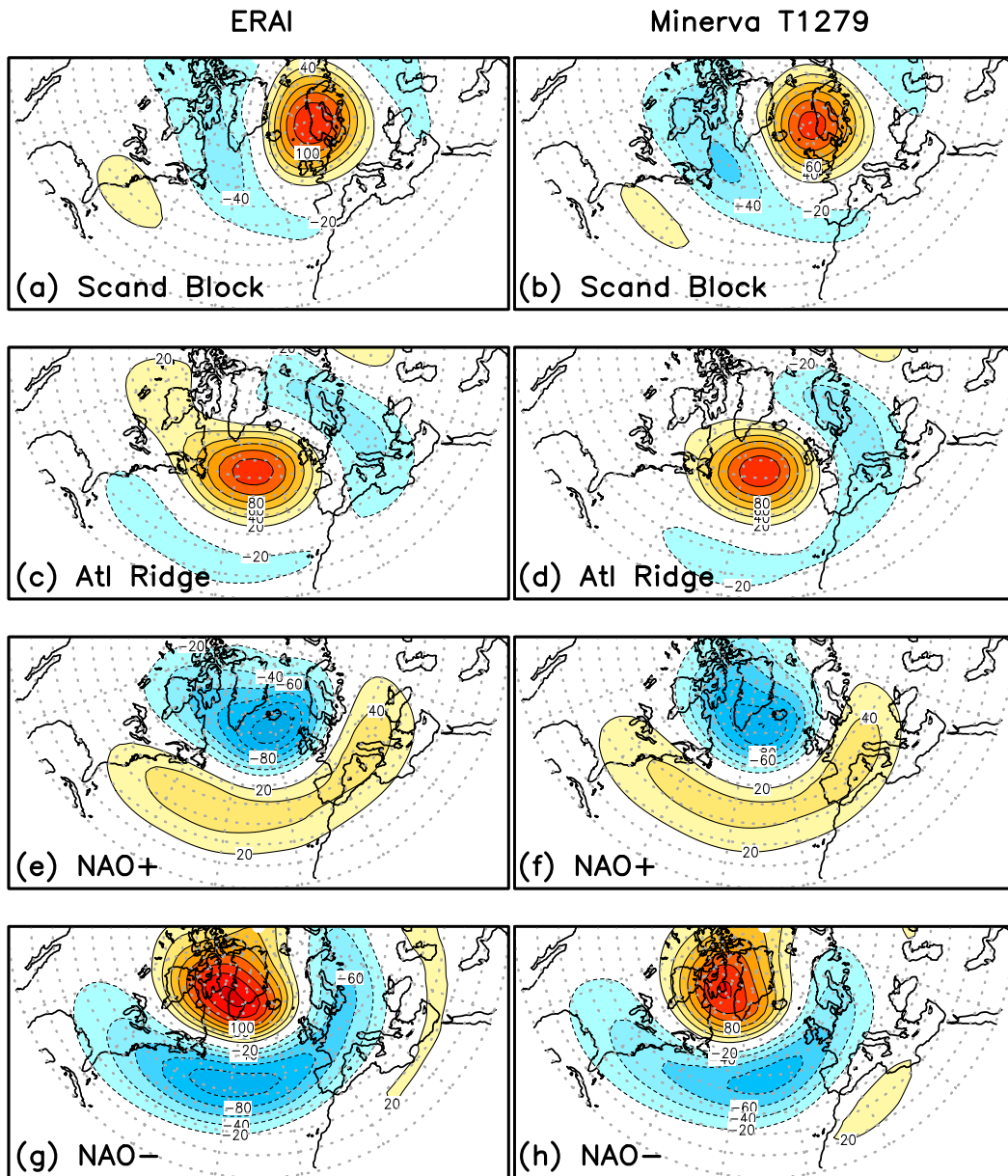


FIG. 4. Anomalous 500-hPa geopotential height (m) for Euro-Atlantic regimes computed for (left) ERA-I and (right) Minerva reforecasts run at T1279 resolution. The domain spans North America, the Atlantic, and Europe ( $120^{\circ}\text{W}$ – $60^{\circ}\text{E}$ ,  $20^{\circ}$ – $90^{\circ}\text{N}$ ). Regimes include (a),(b) Scandinavian blocking, (c),(d) the Atlantic ridge, (e),(f) the positive phase of the NAO, and (g),(h) the negative phase of the NAO.

characterized by anomalous easterlies on its equatorward side with anomalous westerlies on its poleward side (Fig. 5a). The ridge is collocated with a large increase in the frequency of AWB (Fig. 5e). Ridge development is clearly coincident with AWB in the sense that the zonal wind tendency of Fig. 5f is in phase with the anomalous zonal wind in Fig. 5a. Much weaker growth occurs in the absence of AWB (Figs. 5b,d). However, the AWB-related local EP flux divergence

$(\nabla \cdot \mathbf{E})$  indicates that transient eddies work against ridge growth. This suggests that other factors may be more important during development. We have found that ridge decay is assisted by transient eddy forcing during AWB, with comparable contributions from both heat and momentum fluxes (not shown). In the western/central Atlantic, there is a slight eastward shift in CWB (Fig. 5c) toward the region where CWB has a minor role in the growth of the easterlies (Fig. 5d). CWB and

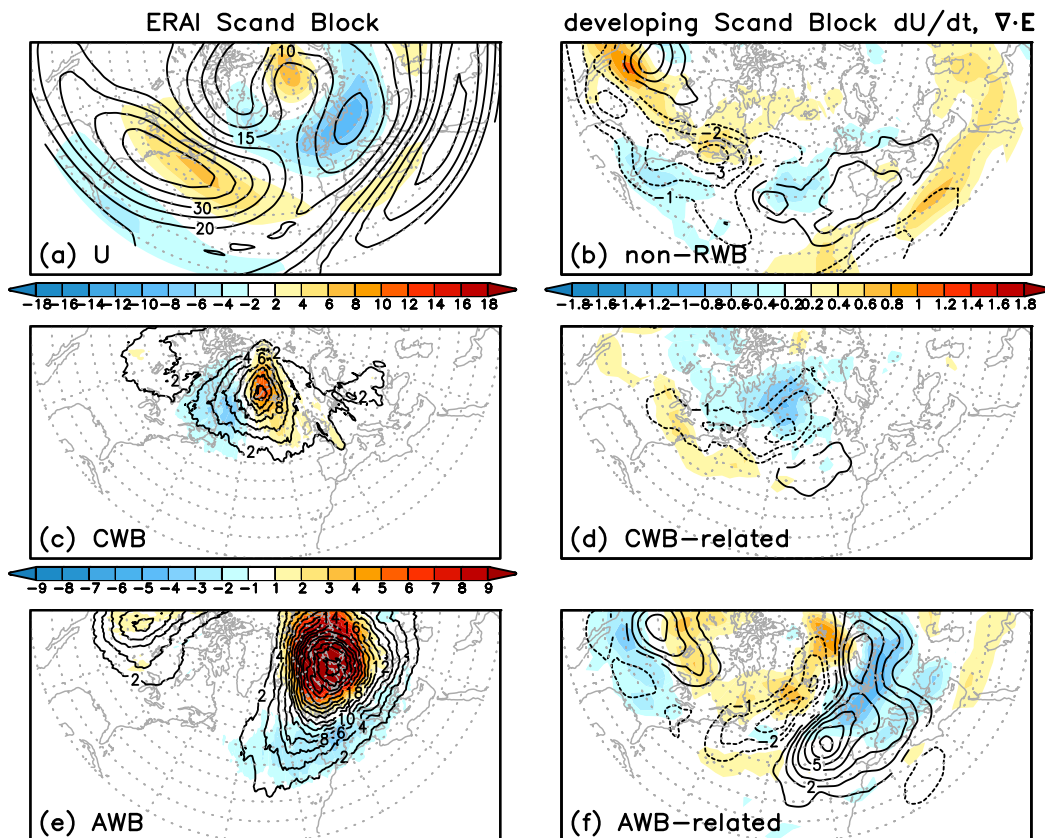


FIG. 5. Total (contours) and anomalous (shading) (a) 250-hPa zonal wind ( $m s^{-1}$ ), frequency (days per season) of (c) CWB and (e) AWB computed during Scandinavian blocking for ERAI. The domain spans North America, the Atlantic, and Europe ( $120^{\circ}W-60^{\circ}E, 20^{\circ}-90^{\circ}N$ ). Note that CWB and AWB frequency is averaged between 315- and 330-K isentropic levels. The divergence of the local EP flux ( $\nabla \cdot \mathbf{E}$ ; contours;  $m s^{-1} day^{-1}$ ) and zonal wind tendency (shading;  $m s^{-1} day^{-1}$ ) at 250 hPa are plotted for the developmental phase, partitioned according to that which is (b) non-RWB, (d) CWB related, and (f) AWB related.

non-RWB variability tend to be more involved during the decay phase (not shown).

The pattern of changes in RWB and corresponding tendencies identified during Scandinavian blocking are simulated reasonably well for Minerva (not shown). Consistent with an underestimation of AWB frequency, the magnitude of the associated zonal wind tendencies is simulated to be weaker than that in ERAI, during both development and decay. Interestingly, this bias is alleviated slightly in Minerva T319 (relative to bias at T1279), which simulates a slightly higher frequency of AWB as well as stronger anomalies in zonal wind itself. However, in general, the role of CWB and AWB is quite similar in all Minerva reforecasts.

*b. Atlantic ridge*

During the Atlantic ridge regime, anomalously high heights span the North Atlantic, while eastern Europe is characterized by low heights (Fig. 4). As with Scandinavian

blocking, the ridge is associated with anomalous westerlies on its poleward flank and anomalous easterlies on its equatorward flank (Fig. 6). The growth of the ridge is coincident with downstream AWB that is much more frequent than normal in the eastern Atlantic (Figs. 6e,f). During AWB, the local EP flux divergence suggests that transient eddy fluxes work to dampen the ridge ( $\nabla \cdot \mathbf{E}$  opposes zonal wind tendency over the central Atlantic) while reinforcing downstream westerlies. As with Scandinavian blocking, it appears that other factors may explain much of the ridge development. CWB exhibits a weak southwestward shift in its frequency of occurrence (Fig. 6c). CWB partly reinforces the easterlies in the western Atlantic and partly counteracts westerlies to the north near Greenland (cf. Figs. 6d and 6a). CWB seems to be more important during decay, during which AWB also plays a significant role in damping the ridge (not shown). These changes are simulated reasonably well for Minerva (not shown); however, zonal wind tendencies associated with RWB during

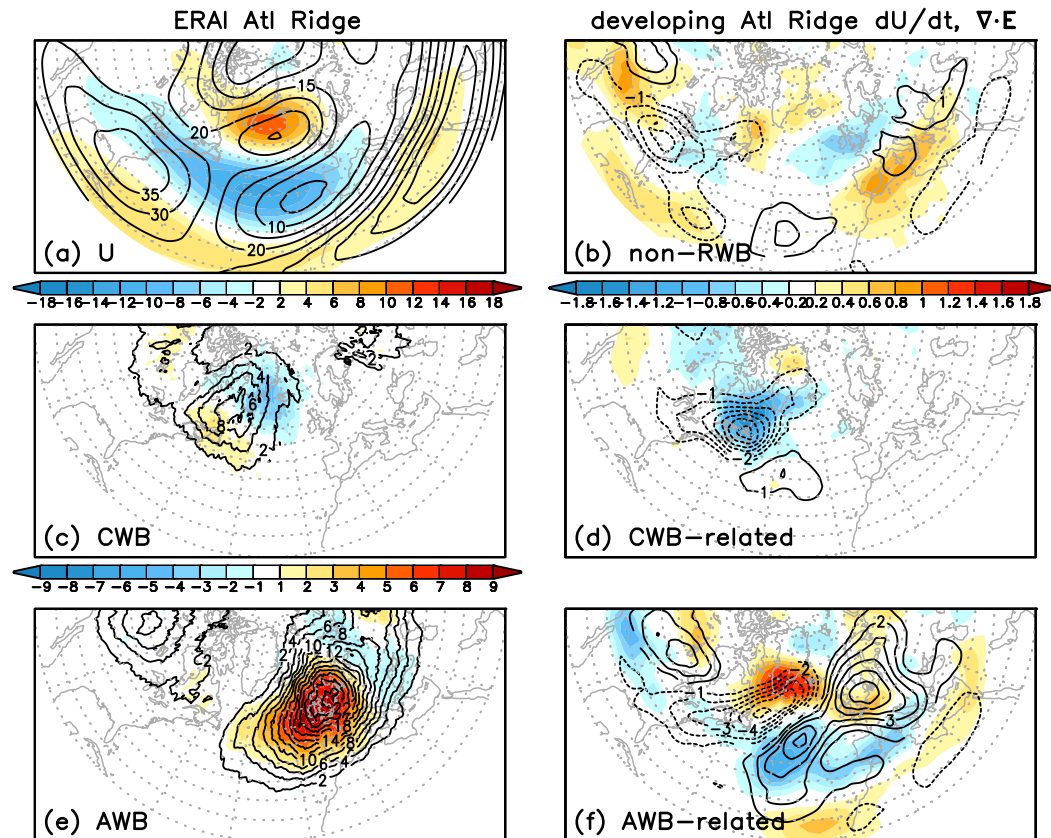


FIG. 6. As in Fig. 5, but for the Atlantic ridge.

development of the Atlantic ridge regime are slightly weaker in the reforecasts.

### c. The positive phase of the NAO

During the NAO+, Greenland and Iceland are covered by anomalously low heights with high heights found farther equatorward, elongated across the Atlantic from North America to Europe (Fig. 4). This is associated with an enhancement/extension of the Atlantic upper-tropospheric jet (Fig. 7). There is a significant decrease in the frequency of CWB (changes at 315 and 330 K reflect roughly a 60% and 90% reduction, respectively) along with an equatorward shift in AWB (Figs. 7c and 7e, respectively). In the western Atlantic, NAO+ development is primarily independent of RWB (cf. shading between Figs. 7a and 7b). In this region, an increase in storminess (not shown) leads to a stronger easterly forcing from transient eddies partly opposing a stronger westerly zonal wind tendency to the north, similar to climatological situation (cf. Figs. 7b and 3a). Farther downstream over the eastern Atlantic, the jet extension is primarily related to AWB and is driven by fluxes from the transient eddies (Fig. 7f). The easterly anomalies to the south are

also linked to AWB but do not appear to be driven by transient momentum and heat fluxes.

Figure 8 shows the zonal wind tendency, the horizontal and vertical components of the EP flux divergence, and the meridional heat flux, averaged across the eastern Atlantic and western Europe and plotted as a function of latitude and pressure. Consistent with the climatological role of AWB (Fig. 8e), here the development of NAO+ is dominated by AWB throughout the depth of the troposphere (Fig. 8f). The AWB-related impact from transient momentum fluxes ( $\nabla \cdot \mathbf{E}_H$ , green contours) is largely in phase with westerly tendencies (shading) at upper-levels. Interestingly, the contribution from heat fluxes ( $\nabla \cdot \mathbf{E}_V$ , black contours) is comparable to that of momentum fluxes at 250 hPa and relatively larger south of 50°N, both in terms of climatological values and during the development of NAO+. This reinforces westerly tendencies but also works against easterly tendencies south of 40°N. This AWB-related maximum in  $\nabla \cdot \mathbf{E}_V$  is related to an increase in poleward heat flux at 200 hPa (maroon contours). If the sign of the meridional wind is considered, it is clear that this feature is primarily due to an equatorward flux of relatively cold air (not shown). This suggests that transient heat fluxes

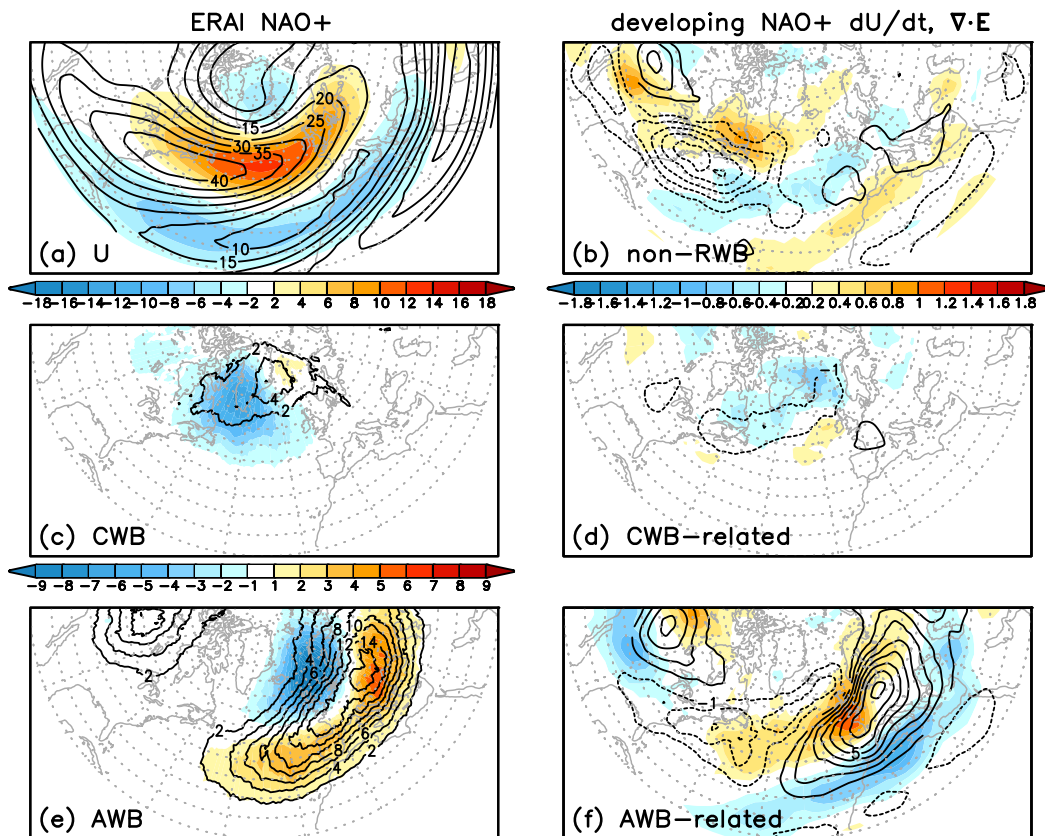


FIG. 7. As in Fig. 5, but for the positive phase of the North Atlantic Oscillation.

play a significant role (via  $\nabla \cdot \mathbf{E}_V$ ) in driving NAO+ development in this region. On the other hand,  $\nabla \cdot \mathbf{E}_V$  tends to work against the zonal wind tendency at 500 hPa during AWB and when wave breaking does not occur (Figs. 8f and 8b, respectively). This effect is strengthened during NAO+ development because of an enhanced and more narrowly confined storm track (not shown). However, it is not reflected in zonal wind tendency, consistent with the barotropic signature of the NAO+.

The frequencies of CWB and AWB during NAO+ are simulated quite well in Minerva T1279 (Fig. 9), as well as for reforecasts at lower resolutions (not shown). However, given an overall underestimation in the climatological frequency in the model, the reduction in the frequency of both CWB and AWB over the North Atlantic during NAO+ development is slightly weaker than the reduction identified in ERAI. Consistent with overall weaker zonal wind tendencies, NAO+ zonal wind anomalies are simulated to be slightly weaker than those in ERAI (cf. Figs. 9a and 7a). In the eastern Atlantic and western Europe, the weaker circulation during NAO+ development is related to what is happening during AWB (Fig. 10). At upper levels, the weaker westerly tendency is consistent with a reduced westerly

forcing induced by relatively less upper-level heat flux (cf. Figs. 10f and 8f). There is also a hint that transient eddy activity independent of RWB is simulated to have less of a destructive impact during NAO+ development (cf. Figs. 10b and 8b).

d. The negative phase of the NAO

During the NAO-, anomalously high heights are found over Greenland along with lower-than-normal heights found equatorward (Fig. 4), in association with a weakening/retraction of the climatological jet (Fig. 11). Note that the NAO- is not exactly equal and opposite to NAO+, and the high heights are shifted northwestward relative to low heights during the NAO+. The NAO- is also closely linked with large changes in RWB frequency, and it coincides with a substantial increase in CWB and decrease in AWB over regions of climatological maxima (Figs. 11c and 11e, respectively). Relative to the climatological frequency of occurrence, CWB is more than doubled, while AWB is greatly reduced at both 315 K and especially 330 K. Considering the climatological zonal wind tendency over the western/central Atlantic, a westerly tendency when CWB is absent (Figs. 12a,e) normally offsets an easterly tendency

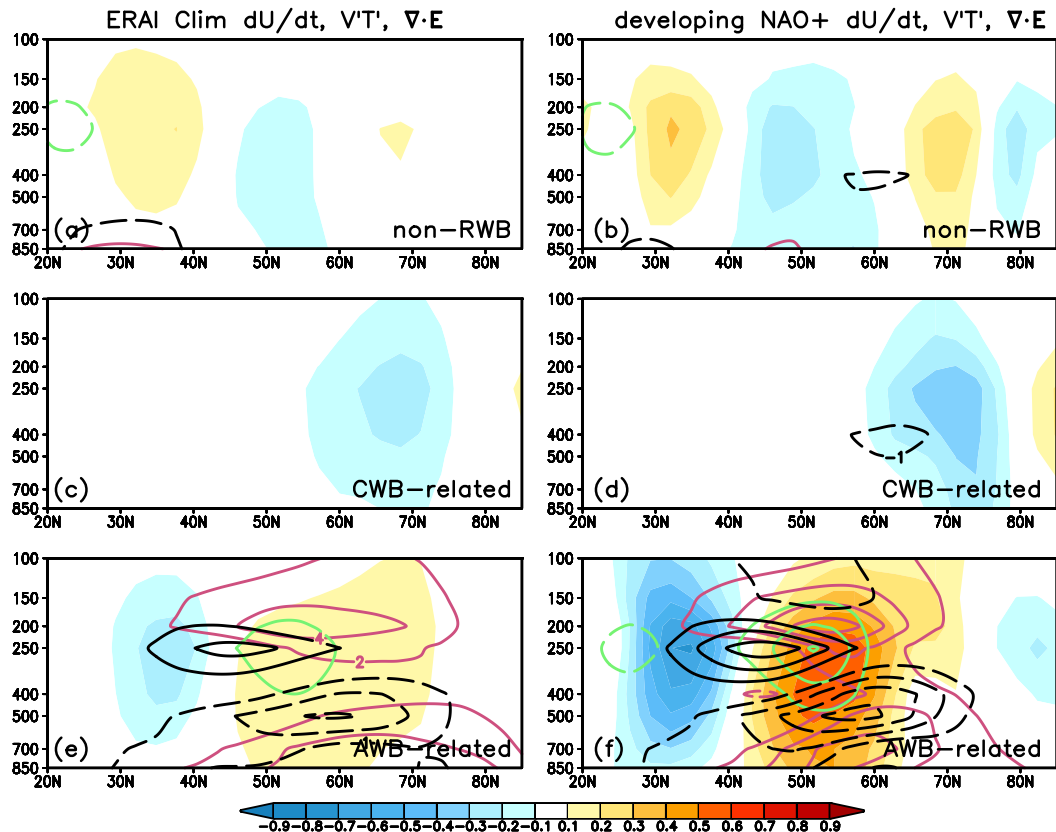


FIG. 8. Tendency of zonal wind (shading;  $\text{m s}^{-1} \text{ day}^{-1}$ ), horizontal and vertical components of the divergence of the local EP flux ( $\nabla \cdot \mathbf{E}_H$  and  $\nabla \cdot \mathbf{E}_V$ ; green and black contours, respectively; intervals of  $1 \text{ m s}^{-1} \text{ day}^{-1}$ ), and meridional heat flux from transient eddies ( $V'T'$ ; maroon contours; intervals of  $2 \text{ K m s}^{-1}$ ) averaged across the eastern Atlantic and western Europe ( $20^\circ\text{W}$ – $40^\circ\text{E}$ ) and plotted as a function of latitude (abscissa) and pressure (ordinate, on a logarithmic scale). Discrete values are defined at the labeled pressure values (at which  $\nabla \cdot \mathbf{E}_H$  and  $\nabla \cdot \mathbf{E}_V$  are also computed). Consistent with Fig. 7, fields are partitioned according to that which is (a),(b) independent of RWB, (c),(d) associated with CWB, and (e),(f) associated with AWB. (left) Climatological values and (right) values during the development of the positive phase of the NAO.

during CWB (Fig. 12c). As noted previously, transient eddies result in a strong easterly forcing that tends to work against the actual westerly wind tendency in the northwestern Atlantic, except during CWB, during which transient eddies reinforce easterlies. It is clear from Fig. 12c that this easterly forcing ( $\nabla \cdot \mathbf{E}$ ) is due primarily to heat fluxes and their resultant vertical gradient ( $\nabla \cdot \mathbf{E}_V$ ). During NAO– development, the growth of zonal wind anomalies appears to be almost entirely related to CWB. The impact of CWB is significantly larger, and the offsetting effect of AWB and non-RWB variability is greatly reduced at around  $60^\circ\text{N}$  (Figs. 12d and 12b, respectively). Transient momentum fluxes involved with CWB largely drive (via  $\nabla \cdot \mathbf{E}_H$ ) the growth of both positive and negative zonal wind anomalies at jet level (250 hPa). Below this (300–500 hPa), easterly tendencies north of  $50^\circ\text{N}$  appear to be primarily related to low-level transient heat fluxes (via  $\nabla \cdot \mathbf{E}_V$ ), which are

preferentially associated with CWB during NAO– development. At the same time, AWB has a weak contribution mainly because of its lack of occurrence.

Results here are consistent with Benedict et al. (2004) and Franzke et al. (2004), who demonstrate that the NAO– regime can be triggered by a single CWB event or maintained by successive events. Our approach of associating variability with RWB fairly accounts for potentially disproportionate impacts of individual RWB events that cannot be inferred from changes in RWB frequency alone.

The NAO– is simulated in Minerva to occur less often than the NAO+; however, the difference in frequency is not as large as that identified in ERAI (Table 1). During the NAO–, the structure of anomalous changes in CWB and AWB frequency is simulated reasonably well in Minerva (Fig. 13), while total frequencies are significantly underestimated (maxima have

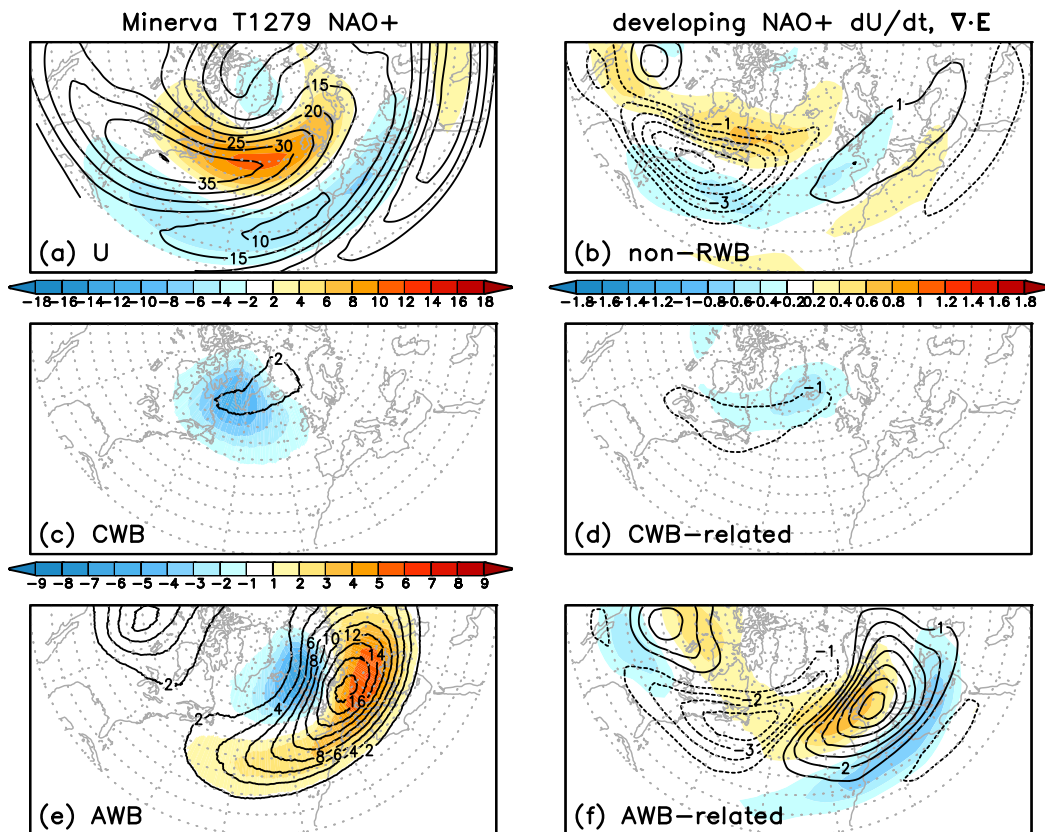


FIG. 9. As in Fig. 5, but for the positive phase of the North Atlantic Oscillation simulated in Minerva reforecasts run at T1279 resolution.

roughly half the magnitude; cf. Figs. 13 and 11). With a lower occurrence, CWB is simulated to have a weaker role in driving the subtropical westerlies during NAO-development (cf. Figs. 13d and 11d), which may explain why the anomalous westerlies are weaker in Minerva than in ERAI. This appears to be largely explained by weaker  $\nabla \cdot \mathbf{E}_H$  (cf. Fig. 14 and Fig. 12). Significantly less storminess is simulated (relative to that in ERAI) in association with CWB, consistent with weaker low-level transient heat flux in Minerva (maroon contours). Altering the heat flux gradient at upper levels, this leads to weaker but vertically broadened EP flux convergence.

### 5. Summary and conclusions

In past studies, the interactive role of Rossby wave breaking (RWB) for the circulation is typically indirectly inferred, and the full impact of the baroclinic transient eddies that are modulated by wave breaking is not generally accounted for. In this study we make a rigorous attempt to quantify the covarying role of RWB in terms of total effect of the transient eddies: the zonal motion driven by *both* momentum and heat fluxes

represented by the divergence of the local three-dimensional Eliassen–Palm (EP) flux ( $\nabla \cdot \mathbf{E}$ ; Trenberth 1986). Nevertheless, the local EP flux divergence does not account for the effect of diabatic heating and friction, and in application to transient eddy fluxes we neglect potentially important low-frequency terms. We use a straightforward approach to partition variability according to that associated with cyclonic wave breaking (CWB), associated with anticyclonic wave breaking (AWB), or considered not directly related to wave breaking (non-RWB).

The interactive roles of CWB and AWP for modifying the eddy-driven jets are examined with primary focus on the North Atlantic. In the western Atlantic, during AWP and in the absence of wave breaking, the impact of transient heat fluxes tends to oppose a strengthening jet to the north (see Figs. 3, 12). This indirectly confirms that other processes are important for climatological jet maintenance, such as low-frequency dynamical effects and especially the mean low-level diabatic heating (Hoskins and Valdes 1990). On the other hand, during CWB the jet is effectively weakened or shifted equatorward, which is partly driven by low to midlevel

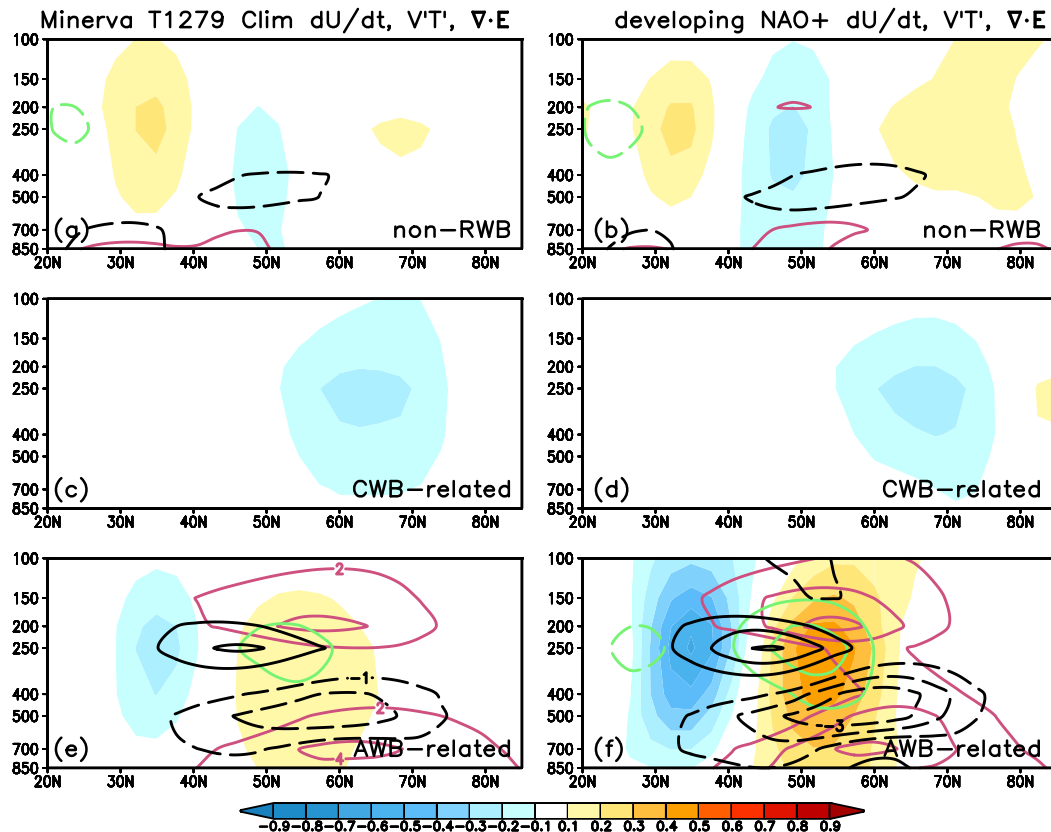


FIG. 10. As in Fig. 8, but for Minerva reforecasts run at T1279 resolution.

transient heat fluxes that act to reduce the vertical shear. This process occurs climatologically and to a larger extent during NAO- development (see Fig. 12). Consistent with the findings of Michel and Rivière (2011), we verify that there is a substantial increase in the frequency of CWB during the development of the NAO-. During the growth of the NAO-, we find that zonal wind tendencies in the western/central Atlantic are almost entirely linked to CWB. Near the tropopause, growth is primarily reinforced by transient momentum fluxes, while transient heat fluxes dominate the forcing of easterlies below the jet in the midtroposphere. AWB has a negligible contribution in the western Atlantic because of its lack of occurrence, and there is a large reduction in AWB farther downstream during the NAO-.

In the eastern Atlantic and western Europe, AWB is most frequent climatologically and has the dominant role of fluxing momentum poleward in the jet exit region (see Fig. 8). The associated westerly wind tendencies are comparably driven by both transient momentum and heat fluxes, reflecting the modulation of the storm tracks by AWB. Interestingly, the upper-level equatorward flux of relatively cold air during AWB significantly

reinforces the enhancement/extension of the Atlantic jet, and to our knowledge this has not been previously noted in the literature. During NAO+ development, transient heat and momentum fluxes also have a comparable role. Because the frequency of AWB is enhanced, both of these AWB-related fluxes play an especially important role during NAO+ development.

Farther upstream over the western Atlantic, NAO+ development is primarily independent of RWB. Despite an enhanced storm track producing additional transient heat fluxes that work to further weaken the jet, other factors such as diabatic heating strengthen the jet on its poleward flank in the absence of wave breaking. In addition, we confirm the substantial reduction in the frequency of CWB during NAO+ development. From the perspective of the anomalous circulation, the lack of CWB is quite important, considering that CWB is normally associated with an easterly tendency that counteracts jet maintenance and extension.

During the development of Scandinavian blocking and the Atlantic ridge, we find a significant increase in AWB frequency coincident with ridge strengthening, both geographically and temporally. However, AWB-related transient eddy forcing does not appear to be

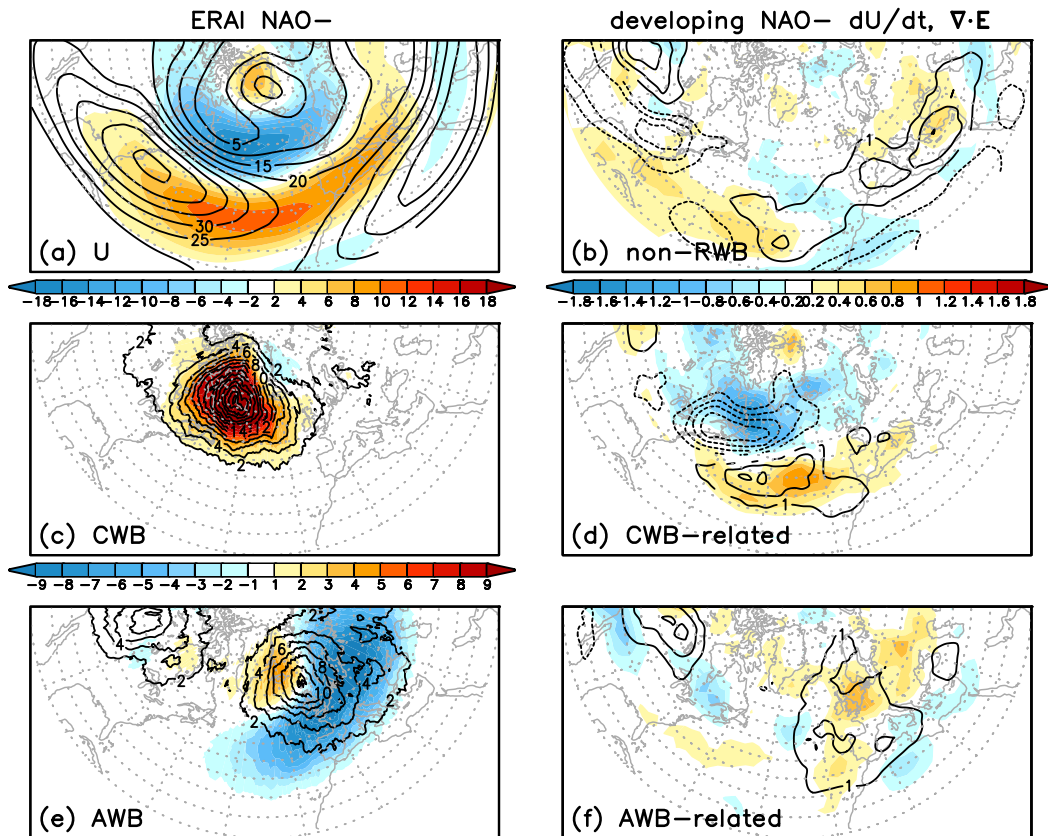


FIG. 11. As in Fig. 5, but for the negative phase of the North Atlantic Oscillation.

driving ridge growth. Comparable contributions from transient momentum and heat fluxes tend to work destructively to either dampen the ridge or push it downstream. Interestingly, this suggests that other factors contribute to ridge growth and blocking. Our finding is consistent with those of Nakamura et al. (1997), who elucidate the barotropic role of low-frequency dynamics as dominant over transient eddy feedback for blocking formation in the Atlantic. During Scandinavian blocking, it is likely that the blocking configuration itself favors AWB without the feedback from transient eddies, and AWB has more of a role during its decay phase.

The roles of CWB and AWB are reproducible in Minerva reforecasts run at all resolutions. However, RWB is generally less effective in driving the circulation, consistent with less frequent wave breaking. Results suggest that this could explain the slightly weaker anomalous flow patterns simulated during both positive and negative phases of the NAO, as well as during Scandinavian blocking.

In this study, the resolution sensitivity of RWB is considered. One might expect a sensitivity of RWB to horizontal resolution, on the theory that resolving small-scale dynamical features improves the larger scales via a

form of upscale energy cascade (Kraichnan 1967; Gkioulekas and Tung 2007). On the contrary, for the range of horizontal resolutions considered (from about 62 km reduced to 16 km), we do not find an improvement in the frequency of either CWB or AWB. Surprisingly, there is even a slight reduction in the frequency of RWB when resolution is increased (becoming less consistent with that in ERAI). We suspect that some kind of dynamical convergence in the simulation of RWB is already attained at the lowest resolution considered here. For a very similar atmospheric model, Jung et al. (2012) demonstrate a clear improvement in the sensitivity of extratropical cyclones, blocking, and even the tropical precipitation and circulation, primarily when horizontal resolution is increased from T159 to T511 (roughly from 126 to 39 km, respectively). It is unclear whether or not this corresponds to an improvement in RWB; however, even if it does, the lowest resolution for the Minerva reforecasts falls within this range.

Last, it should be noted that extratropical cyclones are associated with a great deal of low-level diabatic heating. Given that heating is a direct source or sink of PV depending on the flow configuration, it is plausible that diabatic heating plays a significant role during wave

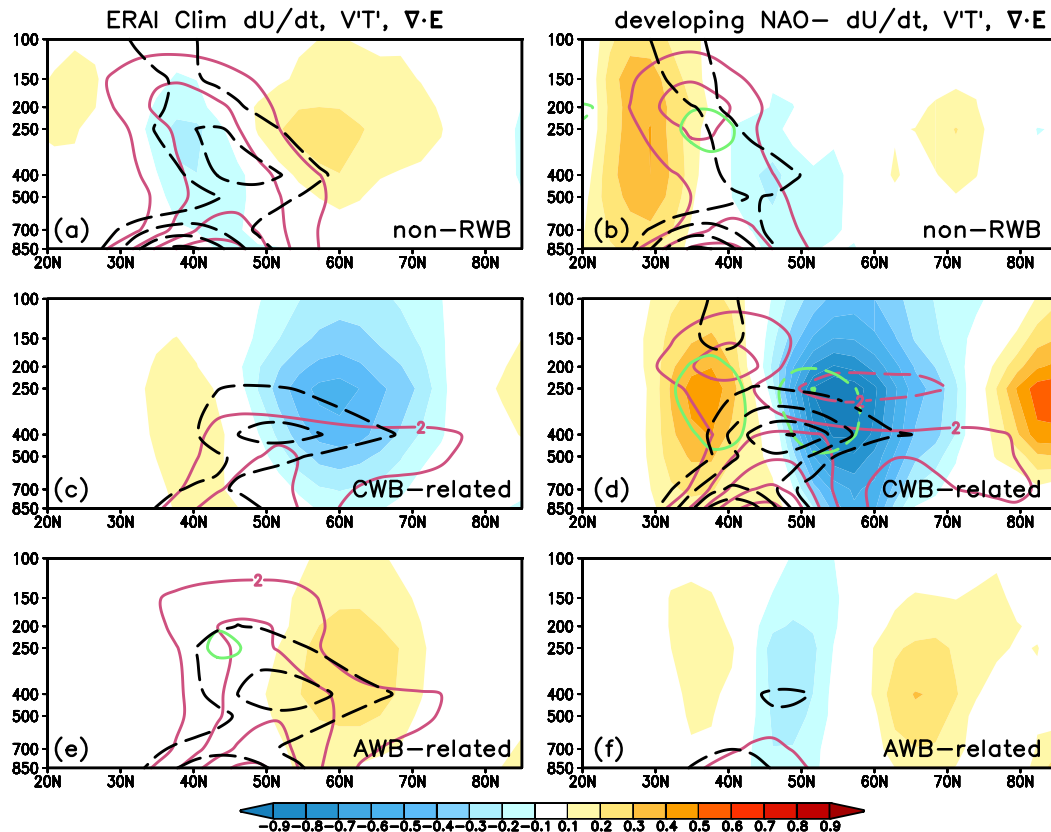


FIG. 12. As in Fig. 8, but for the western/central Atlantic ( $80^{\circ}$ – $20^{\circ}$ W). (a),(c),(e) Climatological values and (b),(d),(f) values during the development of the negative phase of the NAO.

breaking. This is not well understood, and in this study we can only speculate on its role as one factor in the discrepancy between zonal wind tendency and the local EP flux divergence during RWB. Massacand et al. (2001) demonstrate for a particular case study that diabatic heating provides a PV sink that preconditions the circulation prior to an AWB event. A positive feedback is consistent with results shown here. It would be quite worthwhile to further diagnose the impact of diabatic heating alongside fluxes of heat and momentum in a more comprehensive manner. It is unclear how this could be achieved, but it remains an important topic for future study.

*Acknowledgments.* We thank three anonymous reviewers for detailed and helpful comments. This work was supported by the Department of Energy under Grant DE-SC0012599. DMS was also supported by NSF Grant AGS-1338427, NOAA Grant NA14OAR4310160, and NASA Grant NNX14AM19G. We also acknowledge high-performance computing support from Yellowstone (ark:/85065/d7wd3xhc) provided by NCAR's Computational and Information

Systems Laboratory, sponsored by the National Science Foundation.

## APPENDIX A

### Cluster Analysis

Circulation regimes are determined from a cluster analysis based on the  $k$ -means partitioning algorithm. First, principal component analysis is carried out on the low-frequency Z500 fields spanning the Euro-Atlantic (EA)

TABLE 1. Percentage of days that the Euro-Atlantic circulation belongs to each regime cluster (columns) for Minerva T319, Minerva T639, Minerva T1279, and ERAI (rows).

	Scandinavian blocking	Atlantic ridge	NAO+	NAO–
Minerva T319	23	23	31	23
Minerva T639	22	23	29	26
Minerva T1279	21	25	30	24
ERAI	24	25	31	20

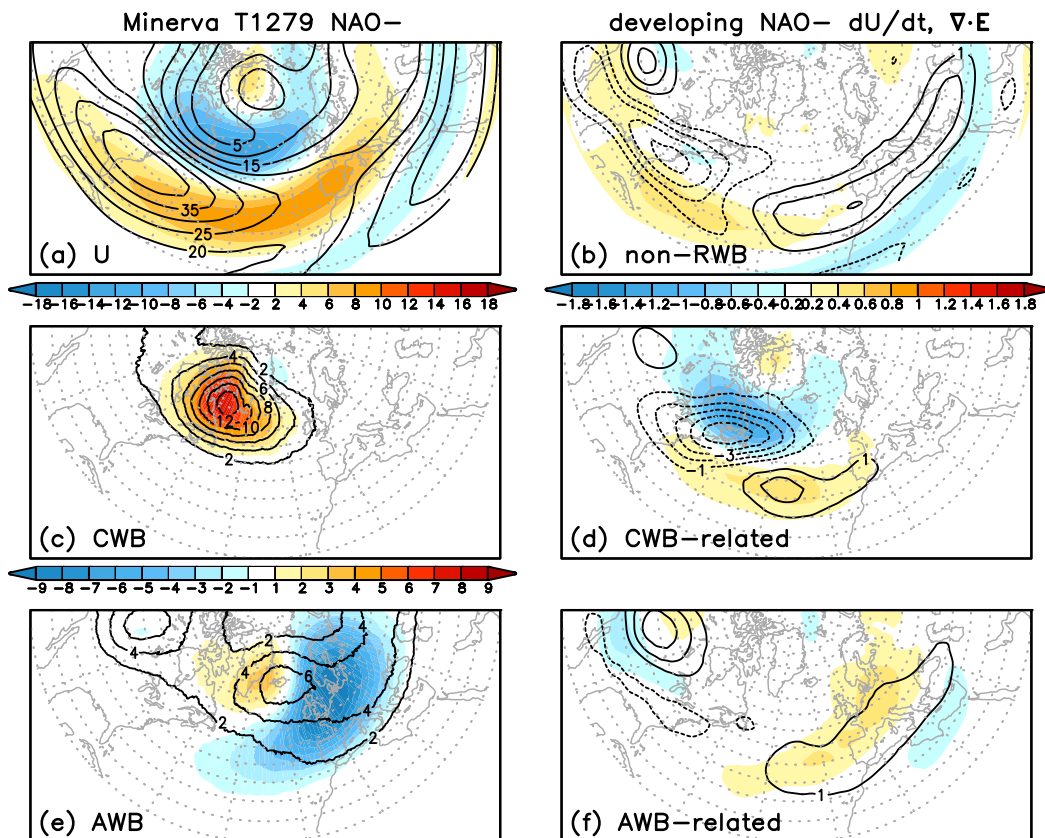


FIG. 13. As in Fig. 5, but for the negative phase of the North Atlantic Oscillation simulated in Minerva reforecasts run at T1279 resolution.

region (see text), with the leading six modes explaining nearly 70% of the total variance. (Increasing the number of modes retained to 12 shows very little change in results.) The partitioning algorithm is carried out on the corresponding principal components (PCs). For a given number of clusters  $k$ , the algorithm assigns each state to a cluster by maximizing the ratio of the variance between cluster centroids (defined by the PC coordinates averaged over all states in that cluster) to the average intracluster variance (spread). The significance of the partitioning for  $k$  ranging from 2 to 6 is determined by comparing the variance ratio obtained from the PCs to those obtained from analysis of a large number (100) of synthetic PC datasets. In each dataset, each PC is generated from a stochastic model that reproduces as much of the lagged autocorrelation structure of the corresponding PC as possible. The percentage of synthetic datasets for which the synthetic variance ratio is less than the actual variance ratio gives a confidence level. The stochastic process used is based on the random phase approximation (Christiansen 2007), as modified by Straus (2010). The autocorrelation of individual PCs for all available lags (given the length of the season) is approximately preserved by this procedure (not shown). The

confidence level tends to increase with  $k$ , so a simple approach is to take the minimum value of  $k$  for which this level exceeds a threshold, here taken to be 0.95. For the EA region,  $k = 4$  achieves this level. Note also that results are robust when using different pressure levels (Vautard 1990).

## APPENDIX B

### RWB Algorithm

The objective computation of RWB partly follows the analysis made by Strong and Magnusdottir (2008) by following circumpolar PV contours at fixed intervals of 0.5 PVU ( $1 \text{ PVU} \equiv 10^{-6} \text{ K m}^2 \text{ kg}^{-1} \text{ s}^{-1}$ ) and identifying areas of sufficient size where the north-south PV gradient reverses, which may be referred to as streamers. This is achieved by considering all areas where relatively low PV intrudes into high PV, with the exception of isolated pockets. Instead of picking the single contour that encloses the largest area (Strong and Magnusdottir 2008), here streamers are defined by the net area spanned by the overturning of at least three contours (a difference of 1 PVU). This ensures the presence of a

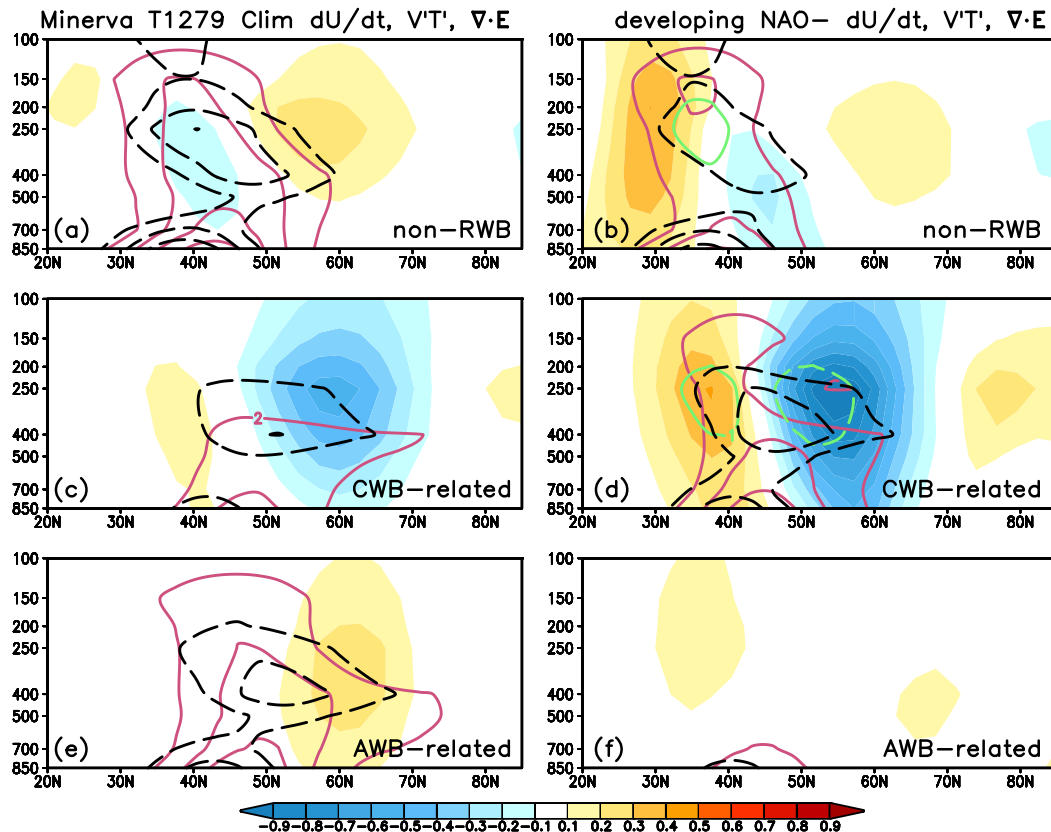


FIG. 14. As in Fig. 12, but for Minerva reforecasts run at T1279 resolution.

strongly reversed gradient, a property typically observed for breaking that tends to occur in the vicinity of upper-tropospheric jets, with weak unrelated overturning ignored. Also, only the longest latitudinal section of reversal is considered at each longitude, and only streamers with an equivalent radius or half zonal extent greater than  $1.25^\circ$  are retained [same as that used by Strong and Magnusdottir (2008)]. Last, for the Minerva reforecasts, weak Gaussian smoothing (using  $\sigma = 0.21^\circ$ , below the resolvable scale of the ERAI grid) is applied to all PV fields prior to applying the detection algorithm, thus removing the possibility of any rectified effects of finescale spatial noise. Nevertheless, note that results are relatively insensitive to either spatial-scale constraint. RWB is designated as cyclonic (CWB) or anticyclonic (AWB) based on the direction of overturning (counterclockwise or clockwise, respectively).

## APPENDIX C

### Association with CWB and AWB

At each location and time (as well as ensemble member for Minerva datasets), a variable is classified according to

one of three components: either it is associated with cyclonic wave breaking (CWB related), associated with anticyclonic wave breaking (AWB related), or independent of wave breaking (non-RWB). For example, if a variable is related to AWB at one location and time, its value at that location and time for the part that is AWB related is the value of that variable, while its value is zero for the part that is CWB related or non-RWB (such that the three components always sum to the total value). Partitioning to either CWB related or AWB related at one location and time is determined based on the distance from that location to the centroid location (average geographic position of all grid points of streamer) of any coincident wave breaking event. For each event, an equivalent radius  $R$  is defined such that the circular area along the surface of a sphere with radius  $R$  is equal to the areal extent of the streamer defining each wave breaking event. Simultaneous fields within a distance of  $4R$  of an event centroid are considered to be related to either CWB or AWB depending on the sign of the event. Attribution is made based on RWB events detected in terms of PV at either 315 or 330 K, or both, and when multiple wave breaking events occur in close proximity, attribution is given to the event with the closest centroid (normalized by  $R$ ).

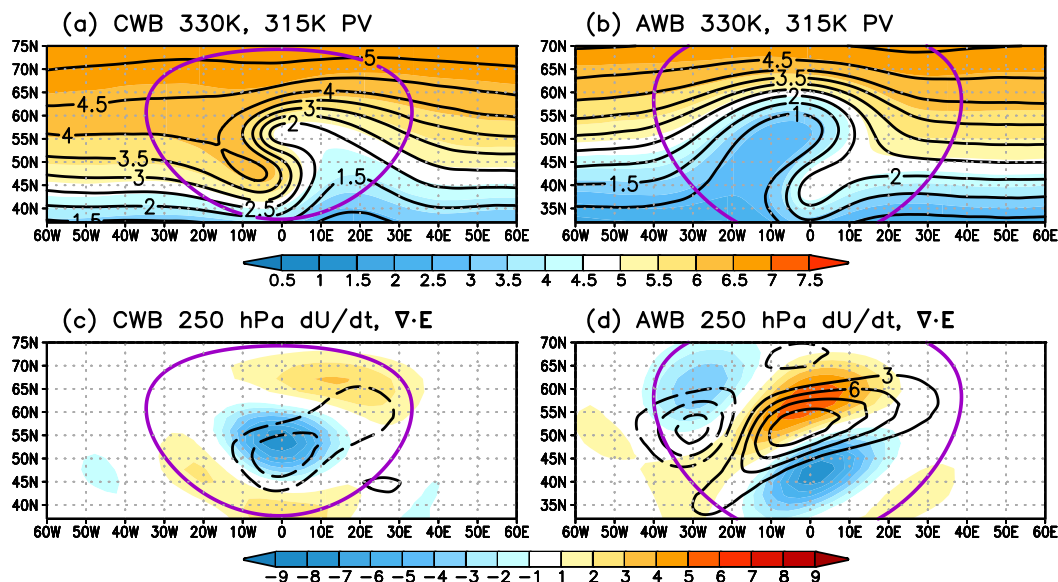


FIG. C1. Wave breaking-centered composites for (a),(c) CWB events detected at 315 K and (b),(d) AWB events detected at 330 K for ERAI. (top) PV (PVU) at 330 (shading) and 315 K (contours). (bottom) Zonal wind tendency (shading;  $\text{m s}^{-1} \text{ day}^{-1}$ ) and divergence of the local EP flux ( $\nabla \cdot \mathbf{E}$ ; contours;  $\text{m s}^{-1} \text{ day}^{-1}$ ) at 250 hPa. Shown in purple is a circle with a radius of 4 times the average equivalent radius. All events with centroids between  $40^\circ$  and  $65^\circ\text{N}$  are used. Longitude and latitude are relative to event centroids, with latitude offset according to average latitude.

Figure C1 shows composites of all CWB and AWB events identified in ERAI, centered according to centroids of individual events. The overturning signature is obvious, and both the zonal wind tendency and the local EP flux divergence ( $\nabla \cdot \mathbf{E}$ ) at 250 hPa exhibit consistency in structure in the vicinity of wave breaking centroids. CWB is characterized by a strong easterly tendency that is reinforced by transient eddies (negative  $\nabla \cdot \mathbf{E}$ ) while westerly tendencies are found to the north and to the south. AWB is characterized by a north–south dipole in zonal wind tendency indicative of poleward movement of the jet, for which westerly tendencies are partly reinforced by transient eddies. Easterly tendencies trail to the west and are offset poleward relative to a region of negative  $\nabla \cdot \mathbf{E}$ . Incorporating the geographic dependence of the frequency of occurrence of CWB and AWB (Fig. 1), the main features in Figs. 3b and 3c bear a resemblance to the event composites in Fig. C1. Disagreement reflects event-to-event differences and the impact of spatial offset. This must account for the negative  $\nabla \cdot \mathbf{E}$  that opposes a positive zonal wind tendency in the northern Atlantic during AWB (Fig. 3c).

A line indicating the boundary of 4 times the average equivalent radius  $R$  is shown in purple in Fig. C1. Normalization by  $R$  is used in order to ensure that, as the area of a wave breaking event goes to zero, the area considered to be related to wave breaking also goes to

zero. However, keep in mind that large-amplitude Rossby waves exhibit systematic planetary-scale structures before breaking is even detected, or when the areal extent of overturning is quite small. After examining results using a range of values for  $n$  for which variables within  $nR$  of a wave breaking centroid are considered to be related,  $n = 4$  is chosen, as it tends to encompass the largest number of grid points for which composite values of zonal wind tendency and  $\nabla \cdot \mathbf{E}$  are significant (based on a Monte Carlo approach) and the least number of grid points for which values are insignificant (not shown). Normalization by  $R$  is consistent with a tendency for the area of significant values to increase with  $R$ . Furthermore, climatological features associated with CWB and AWB (composites of Fig. 3) exhibit far less sensitivity to  $n$  at around  $n = 4$  compared with results for smaller values of  $n$ .

REFERENCES

Balasubramanian, G., and S. T. Garner, 1997: The role of momentum fluxes in shaping the life cycle of a baroclinic wave. *J. Atmos. Sci.*, **54**, 510–533, doi:10.1175/1520-0469(1997)054<0510:TROMFI>2.0.CO;2.

Benedict, J. J., S. Lee, and S. B. Feldstein, 2004: Synoptic view of the North Atlantic Oscillation. *J. Atmos. Sci.*, **61**, 121–144, doi:10.1175/1520-0469(2004)061<0121:SVOTNA>2.0.CO;2.

Cassou, C., 2008: Intraseasonal interaction between the Madden-Julian oscillation and the North Atlantic Oscillation. *Nature*, **455**, 523–527, doi:10.1038/nature07286.

- Christiansen, B., 2007: Atmospheric circulation regimes: Can cluster analysis provide the number? *J. Climate*, **20**, 2229–2250, doi:10.1175/JCLI4107.1.
- Dee, D. P., and Coauthors, 2011: The ERA-Interim reanalysis: Configuration and performance of the data assimilation system. *Quart. J. Roy. Meteor. Soc.*, **137**, 553–597, doi:10.1002/qj.828.
- Drouard, M., G. Rivière, and P. Arbogast, 2015: The link between the North Pacific climate variability and the North Atlantic Oscillation via downstream propagation of synoptic waves. *J. Climate*, **28**, 3957–3976, doi:10.1175/JCLI-D-14-00552.1.
- Franzke, C., S. Lee, and S. B. Feldstein, 2004: Is the North Atlantic Oscillation a breaking wave? *J. Atmos. Sci.*, **61**, 145–160, doi:10.1175/1520-0469(2004)061<0145:ITNAOA>2.0.CO;2.
- , T. Woolings, and O. Martius, 2011: Persistent circulation regimes and preferred regime transitions in the North Atlantic. *J. Atmos. Sci.*, **68**, 2809–2825, doi:10.1175/JAS-D-11-046.1.
- Gkioulekas, E., and K.-K. Tung, 2007: A new proof on net upscale energy cascade in two-dimensional and quasi-geostrophic turbulence. *J. Fluid Mech.*, **576**, 173–189, doi:10.1017/S0022112006003934.
- Holopainen, E. O., L. Rontu, and N.-C. Lau, 1982: The effect of large-scale transient eddies on the time mean flow in the atmosphere. *J. Atmos. Sci.*, **39**, 1972–1984, doi:10.1175/1520-0469(1982)039<1972:TEOLST>2.0.CO;2.
- Hoskins, B. J., and P. J. Valdes, 1990: On the existence of storm-tracks. *J. Atmos. Sci.*, **47**, 1854–1864, doi:10.1175/1520-0469(1990)047<1854:OTEOST>2.0.CO;2.
- Jung, T., and Coauthors, 2012: High-resolution global climate simulations with the ECMWF model in project Athena: Experimental design, model climate, and seasonal forecast skill. *J. Climate*, **25**, 3155–3172, doi:10.1175/JCLI-D-11-00265.1.
- Kraichnan, R. H., 1967: Inertial ranges in two-dimensional turbulence. *Phys. Fluids*, **10**, 1417–1423, doi:10.1063/1.1762301.
- Lau, N.-C., and E. O. Holopainen, 1984: Transient eddy forcing of the time-mean flow as identified by geopotential tendencies. *J. Atmos. Sci.*, **41**, 313–328, doi:10.1175/1520-0469(1984)041<0313:TEFOTT>2.0.CO;2.
- Liu, C., and E. A. Barnes, 2015: Extreme moisture transport into the Arctic linked to Rossby wave breaking. *J. Geophys. Res.*, **117**, 3774–3788, doi:10.1002/2014JD022796.
- Lorenz, E. N., 1963: The mechanics of vacillation. *J. Atmos. Sci.*, **20**, 448–465, doi:10.1175/1520-0469(1963)020<0448:TMOV>2.0.CO;2.
- Machta, L., 1949: Dynamic characteristics of a tilted-trough model. *J. Meteor.*, **6**, 261–265, doi:10.1175/1520-0469(1949)006<0261:DCOATT>2.0.CO;2.
- MacRitchie, K., and P. E. Roundy, 2016: The two-way relationship between the Madden–Julian oscillation and anticyclonic wave breaking. *Quart. J. Roy. Meteor. Soc.*, **142**, 2159–2167, doi:10.1002/qj.2809.
- Manganello, J. V., and Coauthors, 2016: Seasonal forecasts of tropical cyclone activity in a high atmospheric-resolution coupled prediction system. *J. Climate*, **29**, 1179–1200, doi:10.1175/JCLI-D-15-0531.1.
- Martius, O., C. Schwierz, and H. C. Davies, 2007: Breaking waves at the tropopause in the wintertime Northern Hemisphere: Climatological analyses of the orientation and the theoretical LC1/2 classification. *J. Atmos. Sci.*, **64**, 2576–2592, doi:10.1175/JAS3977.1.
- Masato, G., B. J. Hoskins, and T. Woolings, 2013: Wave-breaking characteristics of Northern Hemisphere winter blocking: A two-dimensional approach. *J. Climate*, **26**, 4535–4549, doi:10.1175/JCLI-D-12-00240.1.
- Massacand, A. C., H. Wernli, and H. C. Davies, 2001: Influence of upstream diabatic heating upon an Alpine event of heavy precipitation. *Mon. Wea. Rev.*, **129**, 2822–2828, doi:10.1175/1520-0493(2001)129<2822:IOUDHU>2.0.CO;2.
- McIntyre, M. E., and T. N. Palmer, 1983: Breaking planetary waves in the stratosphere. *Nature*, **305**, 593–600, doi:10.1038/305593a0.
- Michel, C., and G. Rivière, 2011: The link between Rossby wave breakings and weather regime transitions. *J. Atmos. Sci.*, **68**, 1730–1748, doi:10.1175/2011JAS3635.1.
- Michelangeli, P.-A., R. Vautard, and B. Legras, 1995: Weather regimes: Recurrence and quasi stationarity. *J. Atmos. Sci.*, **52**, 1237–1256, doi:10.1175/1520-0469(1995)052<1237:WRRQAQ>2.0.CO;2.
- Molteni, F., and Coauthors, 2011: The new ECMWF seasonal forecast system (System 4). ECMWF Tech. Memo. 656, 51 pp. [Available online at <http://www.ecmwf.int/sites/default/files/elibrary/2011/11209-new-ecmwf-seasonal-forecast-system-4.pdf>.]
- Moore, R. W., O. Martius, and T. Spengler, 2010: The modulation of the subtropical and extratropical atmosphere in the Pacific basin in response to the Madden–Julian oscillation. *Mon. Wea. Rev.*, **138**, 2761–2779, doi:10.1175/2010MWR3194.1.
- Nakamura, H., M. Nakamura, and J. L. Anderson, 1997: The role of high- and low-frequency dynamics in blocking formation. *Mon. Wea. Rev.*, **125**, 2074–2093, doi:10.1175/1520-0493(1997)125<2074:TROHAL>2.0.CO;2.
- Pelly, J. L., and B. J. Hoskins, 2003: A new perspective on blocking. *J. Atmos. Sci.*, **60**, 743–755, doi:10.1175/1520-0469(2003)060<0743:ANPOB>2.0.CO;2.
- Plumb, R. A., 1986: Three-dimensional propagation of transient quasi-geostrophic eddies and its relationship with the eddy forcing of the time-mean flow. *J. Atmos. Sci.*, **43**, 1657–1678, doi:10.1175/1520-0469(1986)043<1657:TDPOTQ>2.0.CO;2.
- Rivière, G., and I. Orlanski, 2007: Characteristics of the Atlantic storm-track eddy activity and its relation with the North Atlantic Oscillation. *J. Atmos. Sci.*, **64**, 241–266, doi:10.1175/JAS3850.1.
- Ryoo, J.-M., Y. Kaspi, D. W. Waugh, G. N. Kiladis, D. E. Waliser, E. J. Fetzer, and J. Kim, 2013: Impact of Rossby wave breaking on U.S. west coast winter precipitation during ENSO events. *J. Climate*, **26**, 6360–6382, doi:10.1175/JCLI-D-12-00297.1.
- Simmons, A. J., and B. J. Hoskins, 1978: The life cycles of some nonlinear baroclinic waves. *J. Atmos. Sci.*, **35**, 414–432, doi:10.1175/1520-0469(1978)035<0414:TLCOSEN>2.0.CO;2.
- Straus, D. M., 1983: On the role of the seasonal cycle. *J. Atmos. Sci.*, **40**, 303–313, doi:10.1175/1520-0469(1983)040<0303:OTROTS>2.0.CO;2.
- , 2010: Synoptic-eddy feedbacks and circulation regime analysis. *Mon. Wea. Rev.*, **138**, 4026–4034, doi:10.1175/2010MWR3333.1.
- , S. Corti, and F. Molteni, 2007: Circulation regimes: Chaotic variability versus SST-forced predictability. *J. Climate*, **20**, 2251–2272, doi:10.1175/JCLI4070.1.
- Strong, C., and G. Magnusdottir, 2008: Tropospheric Rossby wave breaking and the NAO/NAM. *J. Atmos. Sci.*, **65**, 2861–2876, doi:10.1175/2008JAS2632.1.
- Thorncroft, C. D., B. J. Hoskins, and M. F. McIntyre, 1993: Two paradigms of baroclinic-wave life-cycle behavior. *Quart. J. Roy. Meteor. Soc.*, **119**, 17–55, doi:10.1002/qj.49711950903.
- Trenberth, K. E., 1986: An assessment of the impact of transient eddies on the zonal flow during a blocking episode

- using localized Eliassen–Palm flux diagnostics. *J. Atmos. Sci.*, **43**, 2070–2087, doi:[10.1175/1520-0469\(1986\)043<2070:AAOTIO>2.0.CO;2](https://doi.org/10.1175/1520-0469(1986)043<2070:AAOTIO>2.0.CO;2).
- Vautard, R., 1990: Multiple weather regimes over the North Atlantic: Analysis of precursors and successors. *Mon. Wea. Rev.*, **118**, 2056–2081, doi:[10.1175/1520-0493\(1990\)118<2056:MWROTN>2.0.CO;2](https://doi.org/10.1175/1520-0493(1990)118<2056:MWROTN>2.0.CO;2).
- Wallace, J. M., G.-H. Lim, and M. L. Blackmon, 1988: Relationship between cyclone tracks, anticyclone tracks and baroclinic waveguides. *J. Atmos. Sci.*, **45**, 439–462, doi:[10.1175/1520-0469\(1988\)045<0439:RBCTAT>2.0.CO;2](https://doi.org/10.1175/1520-0469(1988)045<0439:RBCTAT>2.0.CO;2).
- Wang, Y.-H., and G. Magnusdottir, 2011: Tropospheric Rossby wave breaking and the SAM. *J. Climate*, **24**, 2134–2146, doi:[10.1175/2010JCLI4009.1](https://doi.org/10.1175/2010JCLI4009.1).
- Zhu, J., and Coauthors, 2015: ENSO prediction in Project Minerva: Sensitivity to atmospheric horizontal resolution and ensemble size. *J. Climate*, **28**, 2080–2095, doi:[10.1175/JCLI-D-14-00302.1](https://doi.org/10.1175/JCLI-D-14-00302.1).